Characterizing the Vulnerability of Flexible Rocking Structures to Strong Ground Motions

M.S. Acikgoz & M.J. DeJong
University of Cambridge, United Kingdom

SUMMARY
Earthquake reconnaissance reports have shown that under the influence of strong ground motions, many flexible structures experience uplift and subsequently exhibit rocking behavior. However, understanding and predicting rocking remains a challenge due to the sensitive dynamic response and the complex interaction of elasticity and rocking. This paper systematically assesses the vulnerability of flexible rocking structures by identifying the earthquake characteristics that cause (i) maximum rocking, and (ii) maximum elastic deformation. Coherent velocity pulses are identified as the driving force of large rocking amplitudes. Using a suite of ground motions where pulses were mathematically expressed and categorized, it is shown that, for large structures, coherent pulses can single-handedly describe the rocking response and are suitable to be used in analysis and design. In most analyses, rocking action was found to isolate the structure from the ground motion, resulting in decreased elastic deformations. However, the inclusion of vertical ground motion in the analyses resulted in 'uplifted resonance', where elastic deformation was magnified.

Keywords: Rocking, Resonance, Near-Field Ground Motion, Vertical Ground Motion, Analytical Dynamics, Dimensional Analysis

1. INTRODUCTION

Independent analytical and experimental works have repeatedly shown the sensitivity of rigid rocking motion to various system parameters. It has been reported that small changes in size, slenderness or the ground motion may result in drastic changes in rocking response (e.g. Aslam et al. 1980). This variance has led to the conclusion that systematic trends can only be observed when the problem is studied from a probabilistic perspective (Chopra and Yim, 1980). Subsequent attempts to deterministically characterize the vulnerability of rocking structures to earthquakes have been futile (Sorrentino et al, 2006). Makris and Roussos (2000) have argued that the randomness of the overturning response can be partially attributed to the fact that the ground motions utilized in earlier studies had no coherent components. Overturning was therefore the result of the interaction of a number of distinct random impulses. However, they suggested that the hidden low frequency pulses in earthquakes are the driving forces of rocking amplification and showed that this was true with several case studies. In recognition, studies which investigate the overturning response to trigonometric pulses followed (e.g. Zhang and Makris 2001). The resulting overturning response is found to be nonlinear but orderly.

In a previous work, the authors of this paper extended the study of Zhang and Makris (2001) to investigate the response of flexible rocking structures to trigonometric pulses. The well-established base isolation characteristic of rocking structures was generally observed to be effective. However, the results also revealed a complex interaction between elasticity and rocking that has the potential to influence patterns of rocking amplification and possibly undermine the base isolation effect (Acikgoz and DeJong, 2012). In this paper, the same idealized analytical model will be used to investigate the

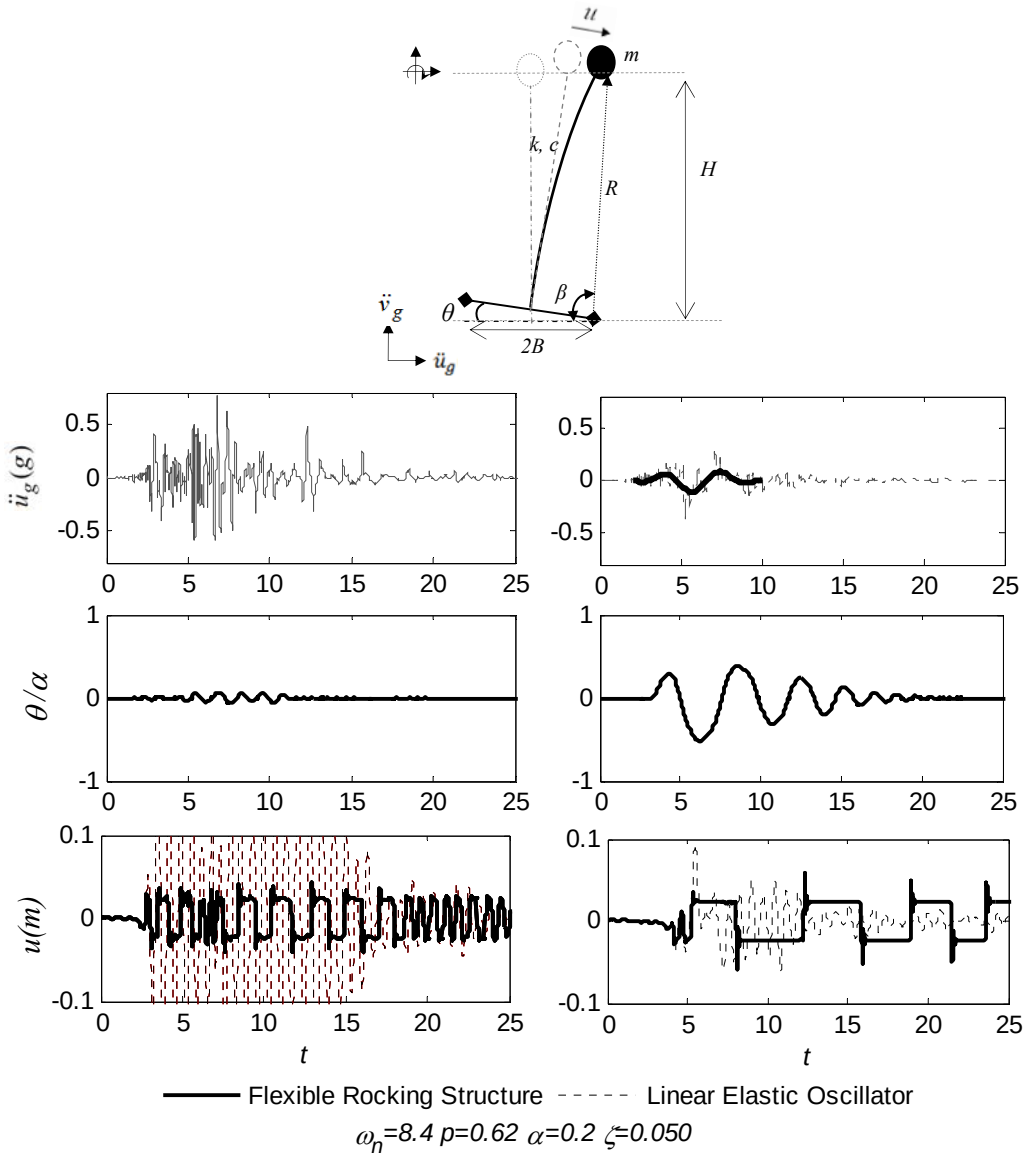

Figure 1.1. (Top) The analytical model of flexible rocking structures and the parameters involved. (Left Column) The acceleration record of Bonds Corner station from the 1979 Imperial Valley earthquake and the rocking and elastic deformation response to this record. (Right) The acceleration record of El Centro Array #4 station from the 1979 Imperial Valley earthquake and the rocking and elastic deformation response to this record.

response to real records in order to define earthquake characteristics that cause maximum rocking and elastic deformation response.

Fig. 1.1 provides the motivation in examining the response to pulse-type records to identify ground motion characteristics which lead to maximum rocking response. Fig. 1.1 (top) shows the analytical model of the flexible rocking structure and its response to two near-field records from the 1979 Imperial Valley earthquake. These records were initially used by Anderson and Bertero (1983) to investigate the response of building type structures to pulse-like earthquakes. Although the first record has a higher peak ground acceleration (PGA), longer effective duration and a more significant resonant response, it cannot sustain rocking motion. Contrastingly, large rocking is observed in the second record which has a pulse-like character. The smooth response indicates that rocking is entirely governed by the coherent pulse, and is largely unaffected by the high frequency oscillation. Upon the termination of the pulse, the rocking action dies away despite the continuing ground motion. Pulses do not seem to illicit an increased elastic response and base isolation can be observed in both cases.

While Fig. 1.1 only exemplifies possible behavior, the objective of this paper is to generalize these observed trends, and to develop practical analysis and design methods for large flexible rocking structures (e.g. bridge piers, frames). It is highly unlikely for such structures to overturn (Huckelbridge and Clough, 1978), so the focus will be on evaluation of the maximum rocking amplitude.

After a review of the equations of motion of the analytical model, the response of a flexible rocking structure to a suite of ground motions will be analyzed. The ability of simple pulse forms to predict maximum rocking deformations will be evaluated, and the limitations of this approach will be discussed. Finally, to determine the ground motion aspects that lead to increased elastic deformations, the effect of vertical ground motions on the deformation response will be investigated.

2. REVIEW OF ANALYTICAL MODEL

An idealized structural model (Fig. 1.1, top) was used to analyze flexible rocking structures (as in Meek 1975, Oliveto et al. 2003). This model assumes that the ground is rigid and that no sliding occurs. The structure is assumed to be a point mass on an axially rigid strut. In Fig. 1.1 (top), the height of the structure is *H*, the base width is 2*B,* and the slenderness is $\alpha = \tan^{-1}(B/H)$. The parameter u is the elastic translation of the mass and θ is the rigid body rotation of the foundation. Alternatively, the response can be defined by *R,* the distance of the lumped mass from the base pivot, and β, the Lagrangian rotation parameter. The classical set of parameters (u,θ) was used in the representation and evaluation of results whereas the Lagrangian set of parameters (R,β) was used in the derivation of the equations of motion and the transition of phases.

There are two phases of the motion of flexible rocking structures: (i) the full contact phase and (ii) the rocking phase. In the full contact phase, the equation of motion is given by:

$$\ddot{u} + 2\zeta\omega_n\dot{u} + \omega_n{}^2 u = -\ddot{u}_g \tag{2.1}$$

where $\ddot{u}_g$ is the horizontal ground acceleration, $\omega_n = \sqrt{k/m}$ is the natural frequency of the system, and $\zeta = c/(2\sqrt{km})$ is the damping factor. A flexible structure with quiescent initial conditions, initially responds elastically until the overturning moment exceeds the resisting moment due to gravity (represented with *g*). Uplift is influenced by the presence of vertical ground acceleration $\ddot{v}_g$, and occurs when:

$$\mp mH(\ddot{u} + \ddot{u}_g) > m(\ddot{v}_g + g)(B \mp u) \tag{2.2}$$

where the upper sign represents rocking about the right base corner and the lower sign about the left base corner. Similar sign notation will be used throughout this paper to represent rocking in each direction. Upon uplift, the rocking phase begins. An important parameter in the response is the frequency parameter, $p = \sqrt{g/R_0}$, which is identical to the natural frequency of a pendulum. This parameter is an indicator of the scale of the structure and therefore provides a measure of resistance to rocking action. The equations of motion for the rocking phase are derived for large rotations and small elastic deformations as:

$$\begin{aligned} \ddot{R} &= \omega_n{}^2 R\left(\frac{B}{\sqrt{R^2 - H^2}} - 1\right) - \frac{2\zeta\omega_n R^2}{R^2 - H^2}\dot{R} + R\dot{\beta}^2 \pm \ddot{u}_g\cos\beta \mp (\ddot{v}_g + g)\sin\beta \\ \ddot{\beta} &= \frac{-2\dot{R}\dot{\beta}}{R} \mp \frac{(\ddot{v}_g + g)}{R}\cos\beta \mp \frac{\ddot{u}_g}{R}\sin\beta \end{aligned} \tag{2.3}$$

These equations are nonlinear, contain coupling between parameters, and are piecewise defined. Different equation sets are valid for $\theta > 0$ and $\theta < 0$, thus at each time step, parameters (R, β) are converted to (u, θ). When $\theta \approx 0$, contact conditions must be assessed to determine the next phase of motion. To do this, both full contact and rocking phases were defined after impact, and the kinetic energy in each was compared to determine which phase governs. Assuming full contact occurs after impact, the body continues its motion deforming elastically. Conservation of angular momentum about the impacting corner yields:

$$\dot{u}_2 = \mp\left(\frac{2B}{R_1}\right)\dot{R}_1 + \left(1 - \frac{B^2 - u^2}{H^2}\right)H\dot{\beta}_1 \tag{2.4}$$

where the upper and lower signs indicate impact on left and right corners respectively, $\dot{u}_2$ is the post-impact full contact velocity, and the subscript 1 indicates pre-impact parameters. After impact, $u_2 = u_1$ and $\theta_2 = \dot{\theta}_2 = 0$. Alternatively, when a rocking phase is assumed to occur after impact, the post-impact parameters of the fictitious rocking phase were derived using a classical impact framework. Assuming inelastic impact without bouncing, and that forces are concentrated on the impacting corner, the post-impact parameters are given as:

$$\dot{\beta}_2 = \left(\frac{H^2 - B^2 + u^2}{{R_2}^2}\right)\dot{\beta}_1 \mp \left(\frac{2HB}{R_1{R_2}^2}\right)\dot{R}_1 \tag{2.5}$$

$$\dot{R}_2 = -\dot{R}_1\left(\frac{R_1}{R_2}\right)\left(\frac{B \pm u}{B \mp u}\right) \tag{2.6}$$

To determine the phase of motion after impact, energies of the rocking and full contact phase, E_r and E_{fc} respectively, are computed and compared. If $E_r > E_{fc}$, a full contact phase follows impact with initial conditions set by Eqn. 2.4. If $E_{fc} > E_r$, a rocking phase is initiated with post-impact parameters given by Eqns. 2.5 and 2.6. These equations of motion and criteria for phase transition describe the dynamic motion of the flexible rocking structure shown in Fig. 1.1.

3. SELECTION AND CATEGORIZATION OF PULSE-TYPE RECORDS

3.1. Selection of Ground Motion Records

To assess the vulnerability of rocking structures to the earthquakes that they are most prone to, a suite of pulse-type records was selected from a list of ground motion records identified as pulse type by Shahi and Baker (2011). The chosen records are from the near-field (R < 25km) and were obtained from the PEER NGA database (Chiou et al., 2004). They have a moment magnitude greater than 5.5 and a peak ground velocity (PGV) greater than 30. The records are from a variety of different geological sites including rock and soft soil conditions. Two of the seven records are from fault parallel components of ground motion.

3.2. Determining Pulse Parameters

Due to the sensitivity of rocking motion to coherent pulses, it is important to identify the amplitude and dominant frequency of the pulse in the earthquake record. To do this consistently, a mathematical model which can emulate the shape of ground motion pulses is required. Furthermore, a versatile mathematical description will aid in categorizing the pulse shapes commonly observed in near-field earthquakes. To capture the long period (coherent) pulse components overridden by high frequency oscillations in acceleration records, it is most convenient to investigate velocity records.

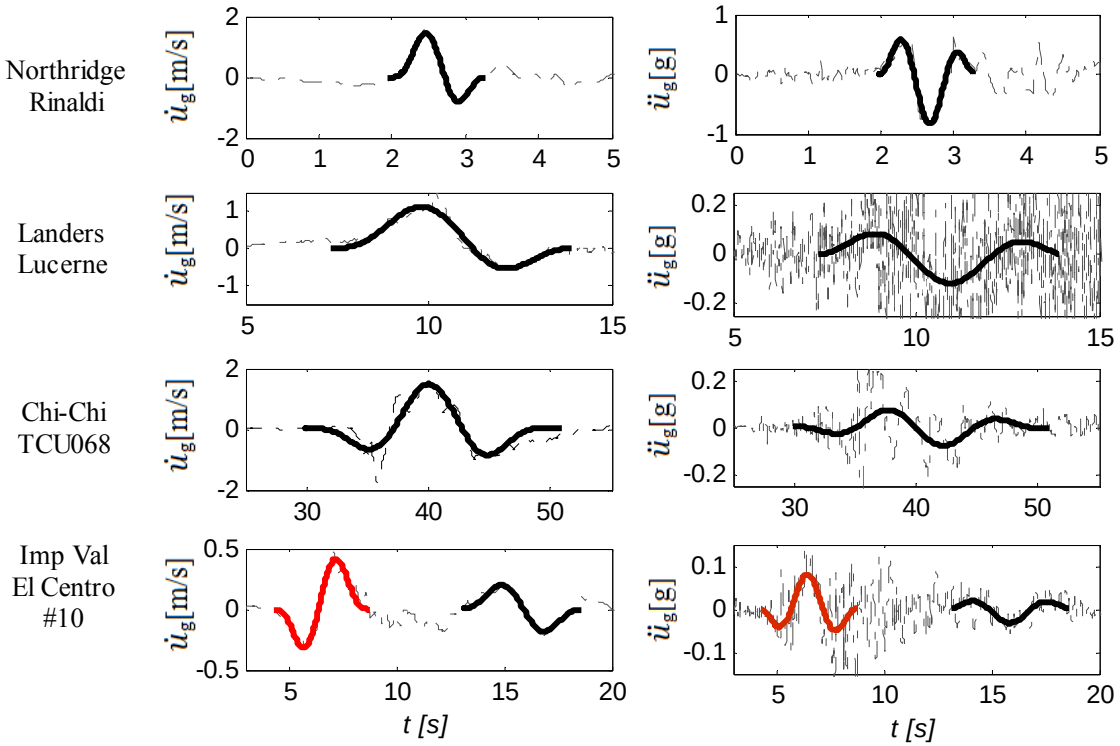

Figure 3.1. Ground velocity and acceleration time histories with fitted M&P wavelets for four pulse-type records.

Ground velocity pulses were extracted using the M&P wavelet (Mavroeidis and Papageorgoui, 2003), which successfully emulates pulses with different ground motion characteristics (Makris and Vassiliou, 2011). The M&P velocity wavelet is described as follows:

$$\dot{u}_g = \begin{cases} \frac{A}{2}\left[1+\cos\left(\frac{\omega}{\gamma}(t-t_0)\right)\right]\cos\left(\omega(t-t_0)+\phi\right), & t_0-\frac{\pi\gamma}{\omega}<t<t_0+\frac{\pi\gamma}{\omega} \\ 0 & otherwise \end{cases} \tag{3.1}$$

where A controls the amplitude of the velocity signal, ω determines the dominant frequency of the wavelet, γ controls the number of significant pulses and ϕ is the phase of the harmonic. Additionally, t_0 indicates the epoch of the envelope and allows the translation of the pulse along the time axis.

An automated nonlinear least squares regression procedure was used to extract pulses from the velocity time history. Fig. 3.1 presents several velocity pulses fitted by this procedure. The corresponding acceleration pulse is presented on the acceleration record. Two parameters e_v and e_a were computed to assess the quality of fit of the optimized pulses to the velocity and acceleration records. These parameters are the adjusted R-squared values and they compare the quality of fit of the nonlinear regression with that of a constant line passing through the mean of the data.

3.3. Categorization of Pulses

In Table 1, important seismological parameters (Moment Magnitude (M_w), Distance to Causative Fault (D), Peak Ground Velocity (PGV), Local Geology (Soil), Faulting Mechanism, etc.) and the fitted pulse parameters are presented for a sub-set of the records used in this study. Previous studies (Bray and Rodriguez-Marek 2004, Mavroeidis and Papageorgoui 2003) have defined attenuation relationships which successfully correlate these seismological parameters to PGV and dominant pulse period. Regression analyses of the suite of ground motions used in this study has revealed that the

Table 3.1 – Sub-set of earthquake ground motion records and fitted pulse parameters

Group	*Earthquake*	M_w	*Station*	*Fault Mech*	*Soil*	*D [km]*	PGV *[cm/s]*	ω *[rad]*	*A [m/s]*	γ	φ	e_v	e_a
1	Northridge	6.69	Rinaldi	R	s	6.5	160	4.69	1.76	1	1.07	0.99	0.89
1	Landers	7.28	Lucerne FP	SS	r	2.2	147	0.82	1.42	0.86	1.08	0.94	0.11
2	Loma Prieta	6.93	Sarotago W Valley FP	OB	s	9.3	62	1.27	0.43	1.9	0.03	0.68	0.09
2	Imperial Valley	6.53	El Centro Array #3	SS	s	12.8	40	1.36	0.31	1.82	0.2	0.91	0.08
2	Chi Chi	7.62	TCU068	OB	s	0.3	177	0.56	1.49	1.85	0.26	0.77	0.15
2	Imperial Valley	6.53	EC Meloland	SS	s	0.1	91	2.26	0.79	1.92	0.27	0.92	0.59
2	Imperial Valley	6.53	El Centro Array #10	SS	s	6.2	48	2.26	0.79	1.92	0.27	0.92	0.59

pulse period can reliably be calculated from $T_p = 2\pi/\omega$ and that there is a strong correlation between PGV and the pulse parameter A (not shown). Therefore, if the local geology and possible fault mechanisms are known, the values of A and ω can be estimated from attenuation relationships. However, there are no relationships available for predicting γ and ϕ, which control the pulse shape.

Statistical analysis of a larger batch of sixty pulse-type records, aimed at correlating γ and ϕ to several earthquake parameters, showed no systematic relationship. Indeed, for earthquakes with non-uniform slip, γ depends on 'the instrument distance relative to the asperities' and therefore is 'difficult to estimate a priori' (Bray and Rodriguez-Marek 2004). To analyze the rocking response to pulse-like earthquakes systematically, records with similar pulse shapes (similar γ and ϕ values) were grouped together. Two example groups of records will be considered herein: Group 1 (γ = 0.75-1.25, ϕ = 60-90º) and Group 2 (γ = 1.75-2.25, ϕ = 0-30º). The different shapes of these records can be seen in Fig. 3.1. Notice that the pulse shapes of the Northridge Rinaldi and Landers Lucerne records are similar, but the former is characterized by forward directivity and the latter is characterized by fling displacement. Aside from the differences in frequency and amplitude of the pulses, note that the abundant noise in the Lucerne Landers acceleration record makes the coherent pulse virtually undetectable.

4. GENERALIZED RESPONSE TO PULSE-TYPE EARTHQUAKES

In this section, the physical similarity of the rocking response to M&P wavelets and pulse-type records will be investigated using dimensional analysis. The objective is to evaluate whether fitted coherent M&P wavelets can describe the response to pulse-type earthquakes single-handedly.

4.1. Physical Similarity of M&P Wavelet Response

It was shown in an earlier study by the authors that the response of flexible rocking structures to trigonometric pulses is physically similar (Acikgoz and DeJong, 2012). This scaling property allowed the representation of results in an intuitive and informative manner for a range of different structures. Here the property of physical similarity will be shown to exist in the response to M&P wavelets using Buckingham's π-theorem. Assuming that the structure is excited horizontally by an M&P wavelet with no vertical component, the response parameter of interest is expressed in terms of the input parameters as follows:

$$\theta = f(\omega_n, \zeta, \alpha, R_0, g, \omega, A, \gamma, \phi, t) \tag{4.1}$$

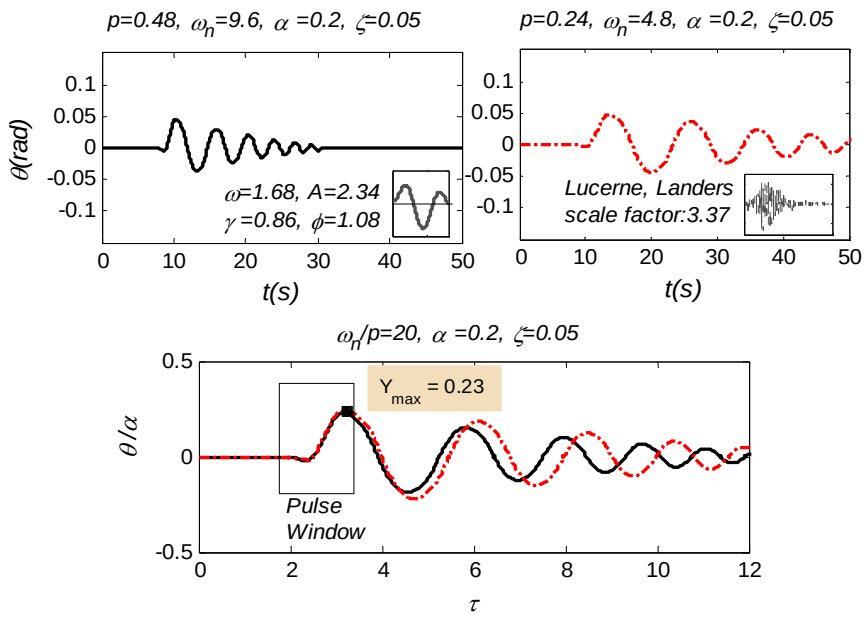

Figure 4.1. (Top) The dimensional response of two different structures to an M&P wavelet and the scaled Lucerne, Landers record and (Bottom) the corresponding non-dimensional response

There are ten input parameters and each of these parameters can be described by two fundamental dimensions of length [L] and time [T]. Therefore eight input parameters are required to describe the dimensionless rocking amplitude:

$$\frac{\theta}{\alpha} = f\left(\frac{\omega_n}{p}, \zeta, \alpha, \frac{\omega}{p}, \frac{A\omega}{g\tan(\alpha)}, \gamma, \phi, \tau\right) \tag{4.2}$$

The dimensionless frequency (ω/p) and strength of excitation ($A\omega/(g\tan\alpha)$) together determine the intensity of the pulse, while γ and ϕ control the pulse shape. Numerical simulations and the simplified non-dimensional form of Eqn. (2.3) show that the system is physically similar when excited with the M&P wavelet (not shown). Therefore, two structures which have different non-dimensional groups (e.g., different ω, A and R_0) but identical dimensionless groups (ω/p and $A\omega/(g\tan\alpha)$), will have exactly the same dimensionless response.

4.2. Physical Similarity of Earthquake Response

In the majority of the pulse-type records listed in Table 1, a dominating coherent pulse is observed early in the time history and the residual components of ground motion are much higher in frequency. Therefore, for large structures which do not 'feel' the high frequency elements of ground motion, long duration pulses may govern the response. To test this hypothesis, the time history response to a ground motion and its fitted pulse can be compared (e.g., DeJong 2012). Additionally, the role of pulses can be generalized further through dimensional analysis. If the pulse shape of a given group of records is similar (i.e. they have the same γ and ϕ) and they are scaled to the same earthquake intensity (ω/p and $A\omega/(g\tan\alpha)$), they should yield a similar dimensionless response. Scaling the intensity of the earthquake without changing the frequency content is possible by adjusting the structural size (p). The amplitude of ground motions can be scaled directly so that the amplitude of the coherent pulse corresponds to the target intensity value.

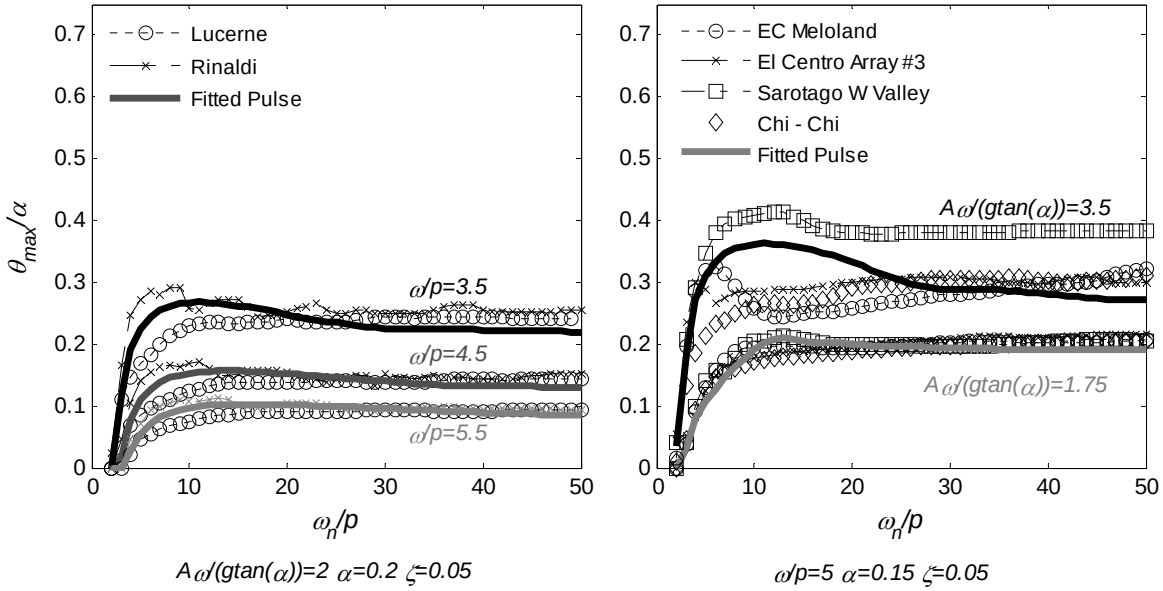

Figure 4.2. Maximum rocking amplitude spectra for different groups of ground motion records under varying earthquake intensities. (Left) Maximum rocking response to Group 1 records with decreasing dominant pulse frequency and (Right) Group 2 records with increasing pulse amplitude. Thick lines indicate response to corresponding M&P wavelets

For example, the non-dimensional responses of two different structures (p = 0.24, 0.48 and ω_n=4.8, 9.6) to the scaled Lucerne Landers record and to an M&P wavelet with the same dimensionless intensity parameters ($\omega/p=3.5$, $A\omega/(g\tan\alpha)=2$), are shown in Fig. 4.1. The good match in the rocking response demonstrates physical similarity, but also that, for sufficiently large structures, coherent pulses alone yielded a good estimate of the maximum rocking deformation.

The dominant effect of pulses can be generalized and evaluated further by comparing different rocking spectra of records with similar pulse shapes. Accordingly, the pulse-like records from Groups 1 and 2 were scaled to different levels of earthquake intensity. The response to these records is compared for structures with different flexibility in Fig. 4.2. The similar shape of the response spectra at each intensity level indicates that the coherent pulse governs the response. The dominance of the pulse is further elucidated by the good spectral match between the fitted M&P wavelets and the different records. The implications of this important result are investigated in the following section.

5. USE OF SIMPLE PULSE FORMS FOR ANALYSIS

5.1. Physical Implications and Limitations

For sufficiently large structures, pulses governed the maximum rocking response, indicating that the emergent time histories prior to the initiation of the pulse are not significant. Prior high frequency oscillations might have caused uplift, but did not sustain rocking motion. Similarly, once the structure was set in motion by the low frequency components, the effect of high frequency pulses was negligible. This can be observed from the smooth outline of the rocking response in Fig 4.1. However, high frequency oscillation near the onset of the low frequency pulse can be important as it can change the instant of uplift, which influences rocking amplification. This is particularly evident for records with $\gamma > 1.5$ (Fig. 4.2, right), where the shapes of the response spectra change with the earthquake intensity.

For some pulse-type records where the coherent pulse coincides with other low frequency pulses, the M&P wavelet might not capture the pulse shape with enough accuracy. In these cases, the quality of

spectral fit might not be good (e.g., Sarotago W Valley record in Fig. 4.2). Also if the structure is not large enough or too slender, the response will be sensitive to high frequency components and the quality of fit would decrease. In this study, $p < 1$ and $\alpha \geq 0.15$ were found to generally meet these size requirements, and the ω/p value of dominant and residual pulses were compared. Records with several low frequency pulses (e.g. Fig. 3.1, bottom row) were not analyzed.

5.2 Defining the Vulnerability using Pulses

This paper identified coherent pulses which are the driving force of rocking amplification and indicates that idealized pulse forms can be utilized instead of actual records to assess the vulnerability of rocking structures to earthquakes. Although pulses govern the response, certain characteristics of the system complicate the interpretation of pulse response and therefore complicate seismic vulnerability predictions. Although dimensional analysis has helped in defining intensity and demand measures, the relationship between these measures remains unclear. Due to sensitivity of rocking amplification and the nonlinearity of response, a higher intensity does not always result in higher rocking amplitudes. This nonlinearity can be observed from the subtle changes in the shape of the response spectrum (see Fig. 4.2). As stated in Section 3.3, the pulse period and amplitude can be predicted reliably, but it is difficult to estimate the pulse shape. The task of the analyst and the designer therefore is to define a pulse shape that would define the worst-case scenario for a given structure. Ongoing work concentrates on defining response spectrum shapes for different levels of earthquake intensity to develop the understanding of vulnerability of rocking structures to earthquakes.

6. ELASTIC DEFORMATIONS AND VERTICAL GROUND MOTION

While the previous sections focus on the maximum rocking amplitude, elastic deformations during rocking are considered briefly here. Once a flexible rocking structure uplifts, an abrupt change is observed in the elastic oscillation frequency and damping; both are significantly increased. Additionally, during rocking most of the energy of the horizontal ground motion is transmitted directly to the rotation of the body. Due to these reasons, rocking provides effective base isolation, and in most cases elastic deformations were significantly smaller than for a similar linear elastic oscillator.

However, results of preliminary analyses of the effects of vertical ground motion on the response show that the vertical component of excitation decreases the efficiency of base isolation by causing significant elastic deformation. This happens for two reasons: (i) the complex interaction of elasticity and rocking, (ii) the high frequency content of vertical ground motions. Contrary to horizontal component of motion, most of the energy of the vertical component is transmitted directly to

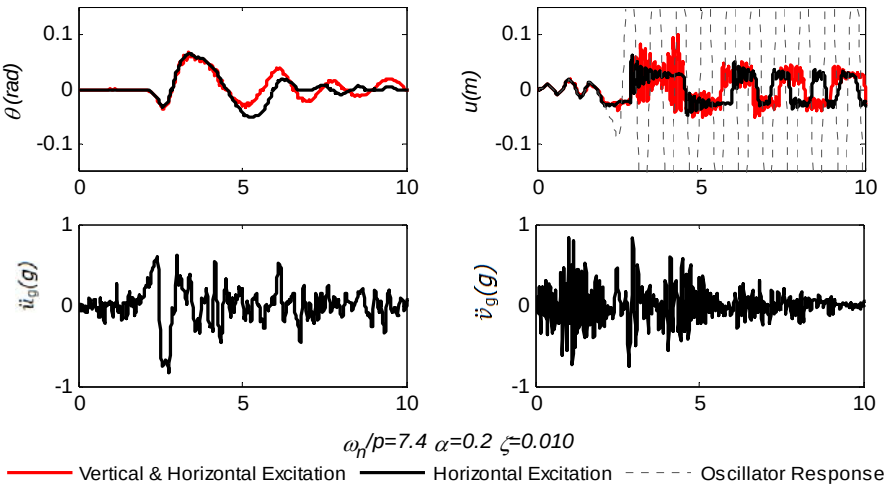

Figure 5.1. The rocking and elastic deformation response of a flexible rocking structure to Northridge Rinaldi record (i) with and (ii) without vertical ground motion.

translational elastic motion. Thus, the characteristic high frequency content of the vertical component of earthquakes can facilitate 'uplifted resonance'. In Fig. 5.1, the rocking and elastic deformation response of a flexible rocking structure to the Northridge Rinaldi record with and without the vertical component is presented. While the elastic deformation behavior is radically different due to aforementioned reasons, the rocking response is similar.

7. CONCLUSIONS

This paper systematically identifies the characteristics of earthquakes that cause maximum rocking amplification and maximum deformation. Coherent pulses were observed to significantly increase rocking response. Therefore, attention was focused on the response to pulse-type records. With the use of dimensional and statistical analyses, it was shown that idealized pulses adequately capture the response of large structures and can effectively replace actual records in analysis and design. The physical interpretation and limitations of this conclusion were discussed. Although base isolation was effective in almost all cases investigated, the vertical component of ground motions was found to decrease effectiveness by facilitating uplifted resonance.

REFERENCES

Aslam, M., Scalise, D. T., & Godden, W. G. (1980). Earthquake rocking response of rigid bodies. *Journal of the Structural Division* **106:2,** 377–392.

Acikgoz, S and DeJong, M.J (2012). The interaction of elasticity and rocking in flexible structures allowed to uplift. *Earthquake Engineering and Structural Dynamics* (published online: **doi**: 10.1002/eqe.2181).

Anderson, J. C. and Bertero, V. V. (1987). Uncertainties in Establishing Design Earthquakes. *Journal of Structural Engineering* **113:8,** 1709-1724.

Bray, J. D. and A. Rodriguez-Marek (2004). Characterization of forward-directivity ground motions in the near-fault region. *Soil Dynamics and Earthquake Engineering* **24:11**, 815– 828.

Chiou, B., R. Darragh, N. Gregor, and W. Silva (2008). NGA project strong- motion database. *Earthquake Spectra* **24:1**, 23–44.

DeJong, MJ (2011). Amplification of rocking due to horizontal ground motion, *Earthquake Spectra* (accepted for publication).

Huckelbridge, A. A. and Clough, R. W. (1978). Seismic response of uplifting building frame. *Journal of the Structural Division* **104:8**, 1211–1229.

Makris, N. and Roussos, Y. S. (2000). Rocking response of rigid blocks under near-source ground motions. *Geotechnique* **50:3,** 243–262.

Mavroeidis, G. P. and Papageorgiou, A. S. (2003). A Mathematical Representation of Near-Fault Ground Motions. *Bulletin of the Seismological Society of America* **93:3**, 1099-1131.

Meek, J. W. (1975). Effects of foundation tipping on dynamic response. *Journal of the Structural Division* **101:7**, 1297–1311.

Oliveto, G., Calio, I. and Greco, A. (2003). Large displacement behaviour of a structural model with foundation uplift under impulsive and earthquake excitations. *Earthquake Engineering & Structural Dynamics* **32:3**, 369-393.

Shahi, S. K. and Baker, J. W. (2011). An Empirically Calibrated Framework for Including the Effects of Near-Fault Directivity in Probabilistic Seismic Hazard Analysis. *Bulletin of the Seismological Society of America* **101:2**, 742-755.

Sorrentino, L., Masiani, R. and Decanini, L. D. (2006). Overturning of rocking rigid bodies under transient ground motions. *Structural Engineering and Mechanics* **22:3**, 293–310.

Vassiliou, M. F. and Makris, N. (2011). Estimating Time Scales and Length Scales in Pulselike Earthquake Acceleration Records with Wavelet Analysis. *Bulletin of the Seismological Society of America* **101:2**, 596-618.

Yim, C. S., Chopra, A. K. and Penzien, J. (1980). Rocking Response of Rigid Blocks to Earthquakes. *Earthquake Engineering & Structural Dynamics* **8:6**, 565–587.

Zhang, J. and Makris, N. (2001). Rocking response of free-standing blocks under cycloidal pulses. *Journal of Engineering Mechanics* **127:5**, 473-483.